Low-frequency unsteadiness in the vortex formation region of a circular cylinder

O. Lehmkuhl, I. Rodríguez, R. Borrell, and A. Oliva

Citation: Physics of Fluids (1994-present) **25**, 085109 (2013); doi: 10.1063/1.4818641
View online: http://dx.doi.org/10.1063/1.4818641
View Table of Contents: http://scitation.aip.org/content/aip/journal/pof2/25/8?ver=pdfcov
Published by the AIP Publishing

PHYSICS OF FLUIDS **25**, 085109 (2013)

Low-frequency unsteadiness in the vortex formation region of a circular cylinder

O. Lehmkuhl,[1,a)] I. Rodríguez,[1] R. Borrell,[2] and A. Oliva[1]
[1]*Heat and Mass Transfer Technological Centre (CTTC), Universitat Politècnica de Catalunya - BarcelonaTech (UPC), ETSEIAT Colom 11, 08222 Terrassa (Barcelona), Spain*
[2]*Termo Fluids S.L., Avda. Jacquard, 97 1-E, 08222 Terrassa (Barcelona), Spain*

(Received 1 February 2013; accepted 31 July 2013; published online 23 August 2013)

The presence of low-frequency fluctuations in the wake of bluff bodies have been observed in several investigations. Even though the flow past a circular cylinder at $Re = 3900$ ($Re = U_{ref}D/\nu$) has been the object of several experimental and numerical investigations, there is a large scattering in the average statistics in the near wake. In the present work, the flow dynamics of the near wake region behind a circular cylinder has been investigated by means of direct numerical simulations and statistics have been computed for more than 858 shedding cycles. The analysis of instantaneous velocity signals of several probes located in the vortex formation region, point out the existence of a low-frequency fluctuation at the non-dimensional frequency of $f_m = 0.0064$. This large-scale almost periodic motion seems to be related with the modulation of the recirculation bubble which causes its shrinking and enlargement over the time. Two different configurations have been identified: (i) a high-energy mode with larger fluctuations in the shear-layer and in the vortex formation region (Mode H) and (ii) a low-energy mode with weaker fluctuations in the shear layer (Mode L). The influence of such a low-frequency in the wake topology has been studied not only by means of the phase-average flow field for each mode, but also by the analysis of the time-average first- and second-order statistics of each wake mode. The results are compared with the long-term averaged solution and with results in the existing literature. © *2013 AIP Publishing LLC*. [http://dx.doi.org/10.1063/1.4818641]

I. INTRODUCTION

The flow over a circular cylinder has been the subject of many numerical and experimental studies. From a theoretical point of view, it has been considered a canonical case for performing studies about the behaviour of the separated shear-layers, transition to turbulence, and the interaction between shear-layers and the turbulent wake. On the other hand, this case is also of interest since the flow around cylindrical structures is of relevance for many practical applications, e.g., heat exchangers, bridge piers, chimneys, towers, antennae, wires, etc. The knowledge about flow-related unsteady loading of such structures is crucial for hydro and aerodynamic control and design.

As it is well known from experimental observations, the flow around a circular cylinder exhibits different behaviours depending on the Reynolds number.[1,2] In the range of Reynolds numbers between $40 < Re < 10000$ ($Re = UD/\nu$, based on the free-stream velocity U and the cylinder diameter D), Roshko[1] observed different regimes: (i) a stable range characterised by laminar vortex shedding for $40 < Re < 150$; (ii) a transition regime in the range $150 < Re < 300$ with irregular bursts of the velocity in the wake; and (iii) an irregular regime for $300 < Re < 10000$ where transition occurs in the separated shear layers. These observations were later confirmed by Bloor[2] and Williamson.[3]

[a)]Also at Termo Fluids S.L., Avinguda Jacquard, 97 1-E, 08222 Terrassa (Barcelona), Spain. Electronic mail: cttc@cttc.upc.edu.

In fact, Williamson[3] found that the transition to three-dimensional flow is characterised by two discontinuous changes. The first one at about $Re \sim 190$, whereas the second one was found to occur at about $Re \sim 260$. The latter (also named as mode B instability[4]) shows finer-scale stream-wise vortex pairs. With increasing Reynolds number, the three dimensional cylinder wake becomes more chaotic and finally, at Reynolds number around 1200 the shear layers separating from the cylinder become unstable.[5] At Reynolds number 5000, there is an abrupt change in the appearance of the vortex shedding initially found by Norberg[6] and later confirmed by Prasad and Williamson.[7] This transition involves the inception of vortex dislocations. The wake topology remains unchanged up to Reynolds number 2×10^5. Then, a dramatic decrease in the drag coefficient occurs between Reynolds numbers 2×10^5 and 5×10^5, named critical regime by Roshko.[8] In the critical regime, there are two discontinuous drops in the drag and the existence of asymmetric forces on the cylinder surface.[9,10] Another transition occurs in the range $10^6 < Re < 3.5 \times 10^6$, with the drag increasing again.[8,10] At post-critical Reynolds numbers beyond 3.5×10^6, the boundary layer at the cylinder becomes turbulent before separation (see for instance Ref. 8).

The case at $Re = 3900$ has been extensively investigated (e.g., Refs. 11 and 12 and the citations therein). However, in spite of the many studies carried out, there is a large scattering in the mean flow solutions in the near wake (see Figure 9 in Ref. 12) which seems to converge into the same solution as the flow moves downstream. These differences in the near wake have been identified with different mean flow configurations of the stream-wise velocity usually referred to as U-shape and V-shape profiles. According to Ma *et al.*[11] both states reflect the dynamics of the flow in the very near wake which is very sensitive to disturbances. They concluded that U-shape profile emerges if the background fluctuations are relatively low or the span-wise extent of the domain is small ($L_z/D \leq \pi$, here L_z stands for the span-wise size).

However, the observations of Ma *et al.*[11] are in disagreement with the results of other investigations where $L_z/D = \pi$ was also used. Breuer[13] by means of large-eddy simulations (LES) computed this flow using different subgrid-scale (SGS) models and span-wise resolutions. Owing to the length of the recirculation bubble obtained with the finest grid, his solution yielded a V-shaped profile. Kravchenko and Moin[14] with $L_z = \pi D$, almost simultaneously to the studies of Ma *et al.*,[11] computed a recirculation length in between both solutions identified by Ma *et al.*,[11] thus obtaining a quasi V-shaped profile. Franke and Frank[15] showed that average statistics in the wake of the cylinder would require a large integration time. They presented results for about 200 time-units but commented that it was not enough for obtaining converged statistics. Yet, they pointed out that their solution approached that of Ma *et al.*[11] for the corresponding span-wise width ($L_z/D = \pi$). Tremblay *et al.*[16] by means of direct numerical simulations (DNS) and using a span-wise size of πD obtained the characteristic V-shape profile (with 300 time-units of time integration) contradicting the hypothesis of Ma *et al.*[11] about the span-wise size. Indeed, they observed that the shape of the stream-wise velocity profile developed from U towards V as long as the recirculation length was not settled down to a stable state. More recently, Parnaudeau *et al.*[12] performed experimental and numerical studies and found, by analysing their low-resolution LES results, that about 1200 time-units (250 shedding cycles) were required for obtaining a converged value for the mean recirculation length. In their case, the obtained solution showed a U-shaped stream-wise velocity profile.

All these studies pose the question about how the unsteady behaviour of the vortex formation region affects the near wake configuration. (Here, the vortex formation region is defined as the location downstream the cylinder where the root-mean-square of the stream-wise fluctuating velocity component reaches a maximum at the wake centreline,[4,17] whereas the mean recirculation region closes at the location with zero time-average velocity at the wake centreline.) However, to the best of our knowledge, there is no complete study of the convergence of flow statistics in the very near wake. On the other hand, low-frequency variations in the wake of bluff bodies have been observed by several investigations. Berger *et al.*[18] studied the formation of coherent structures in the wake of a disk and a sphere at Reynolds numbers between $1.5 \times 10^4 < Re < 3 \times 10^5$, and found what they called a pumping mechanism of the recirculation bubble with a very low-frequency. In the case of the sphere, the existence of such low-frequency modulation was observed in the energy spectra from numerical experiments of Tomboulides and Orszag,[19] but recently has been also measured by means

of DNS at $Re = 3700$ by Rodríguez *et al.*[20] Najjar and Balachandar[21] also observed a low-frequency unsteadiness in the wake of a normal flat plate, finding a high-drag regime with high coherence in the span-wise vortices and a low-mean drag regime where less coherent vortices were formed. Later, Miau *et al.*[22] found such variations in the wake of a trapezoidal cylinder and a circular cylinder at Reynolds numbers above 10^4 and showed that they were associated with the unsteady variations of the vortex formation length. Wu *et al.*[23] studied the low-frequency fluctuations of the wake behind a normal plate confirming the existence of the two modes pointed out by Najjar and Balachandar,[21] but at the Reynolds numbers of their experiments they found an asymmetry in the time where these modes occurred. In fact, they detected that the most energetic one, with a shorter vortex formation region, only occurred during the 5% of the total measured time.

Such a low-frequency fluctuation mechanism might be responsible for the large scattering of the statistical data in the wake of the circular cylinder, but this issue appears to be still open. This paper reports on the detection of low-frequency unsteadiness of the vortex formation region past a circular cylinder at $Re = 3900$. Thus, the main focus of this work is on the low-frequency modulation of the recirculation zone, to examine its possible influence on the wake configuration, as well as to derive more time-accurate flow parameters and first- and second-order statistics. In this work, we perform a comprehensive time series analysis by utilising data from several probes located at different stations in the shear-layers and in the near wake. By means of the analysis of the power spectra of these probes, the co-existence of two different wake configurations which alternate at very low-frequency has been found. In order to study the influence of such low-frequency in the wake topology, the phase-average flow field for each mode has been computed. After that, time-average first- and second-order statistics of each wake mode have been compared with the long-term averaged solution (of about 4000 time-units) and with available results in the literature.

II. DESCRIPTION OF NUMERICAL METHOD

The methodology used for solving the flow over bluff bodies with massive separation is described in Rodríguez *et al.*[20,24] The governing equations have been discretised on a collocated unstructured grid arrangement, by means of second-order symmetry-preserving schemes.[25] Such schemes are conservatives, i.e., they preserve the symmetry properties of the continuous differential operators, and ensure both stability and conservation of the global kinetic-energy balance on any grid. For the temporal discretisation of the momentum equation a two-step linear explicit scheme on a fractional-step method has been used for the convective and diffusive terms,[26] while for the pressure gradient term an implicit first-order scheme has been used.

The three-dimensional (3D) meshes used for solving the domain considered have been generated by the constant step extrusion in the homogeneous direction of a two-dimensional (2D) unstructured grid. Under these conditions, the span-wise coupling of the discrete Poisson equation, which results from the incompressibility constraint, yields circulant sub-matrices that are diagonalisable in a Fourier space. This allows the Poisson equation to be solved by means of a Fast Fourier Transform (FFT) method. The algorithm used is based on the explicit calculation and direct solution of a Schur Complement system for the independent 2D systems. For more details, readers are referred to Borrell *et al.*[27]

III. PROBLEM DEFINITION AND COMPUTATIONAL DOMAIN

The DNS of the flow past a circular cylinder at $Re = 3900$ is considered here. The case has been solved using a computational domain of dimensions $[-8D,16D]$; $[-10D,10D]$; and $[0,\pi D]$ in the stream-, cross-, and span-wise directions, respectively, with a circular cylinder of diameter D at (0,0,0). As for the span-wise size of the domain, it was shown in a previous study[28] that there was no influence in the statistical data when the span-wise size of the domain was doubled. A detailed comparison of averaged first- and second-order statistics considering a larger span-wise size is given in Appendix A. As the main concern of the present work is about the low-frequency variations in the near wake and on the time-dependence of turbulent statistics, a large integration time is required.

Hence, considering the results, the computational effort has been focused on the long-term average statistics instead of a larger span-wise domain.

The boundary conditions consist of a uniform velocity (u,v,w)=(1,0,0) at the inflow, slip conditions in the top and bottom boundaries of the domain, and a pressure-based condition at the outlet of the domain. At the cylinder surface, a no-slip condition is prescribed. As for the span-wise direction, periodic boundary conditions are imposed. As mentioned before, the governing equations are discretised on an unstructured mesh generated by the constant-step extrusion of a two-dimensional unstructured grid. The use of an unstructured grid for the plane has allowed to cluster more control volumes around the cylinder surface and in the near wake. The results presented throughout this paper are computed with a grid of about 9.3 million control volumes (CVs), 72700 $\times$ 128 planes. In *a posteriori* analysis of the grid size used, we have calculated the Kolmogorov length scale which gives $\overline{\eta}/D = 0.02$ on average in the near wake ($x/D < 5$). In this zone, the average grid size is about $\overline{h}/D = 0.018$, yielding a ratio $\overline{h}/\overline{\eta} = 0.9$. With this ratio between grid-size and Kolmogorov scale, the resulting grid density obtained should be fine enough for solving the smallest flow scales in the near wake.

IV. RESULTS

The simulations have been started from homogeneous flow and initially, some random perturbations have been introduced. In order to ensure a temporal converged statistically steady state, the flow field has been advanced in time for an initial duration of 75 tU/D. Once the initial transient has been washed out, statistics have been collected and averaged over approximately 3900 tU/D, which is about 836 shedding cycles. This time integration results in a long simulation time and is by far the largest numerical experiment carried out at this Reynolds number for this flow. This large integration time should ensure not only converged statistics but also a large time span to analyse the existence of low-frequency variations in the vortex formation region. It should also be pointed out, that first- and second-order statistics presented have been averaged both in time and in space (in the span-wise direction).

A. Energy spectrum

Single-point measurements have been carried out by positioning probes at different locations. Measurements at those ports have been taken over the whole simulation time. The location of these stations is as follows: $P1 \equiv [x/D = 0.71, y/D = 0.66]$ and $P2 \equiv [x/D = 1.3, y/D = 0.69]$ are located in one of the shear-layers, $P3 \equiv [x/D = 2.0, y/D = 0.0]$ and $P4 \equiv [x/D = 3.0, y/D = 0.0]$ are located in the wake centreline, $P5 \equiv [x/D = 2.0, y/D = 0.59]$ in the wake, $P6 \equiv [x/D = 0.5, y/D = 0.0]$ at the cylinder base, and $P7 \equiv [x/D = -0.171, y/D = 0.465]$ quite close to the laminar boundary layer at about 70° from the stagnation point (see Figure 1).

The main frequencies corresponding to the large-scale vortex shedding (f_{vs}) and the small-scale Kelvin-Helmholtz (KH) instabilities of the shear-layers (f_{KH}) have been obtained from the power

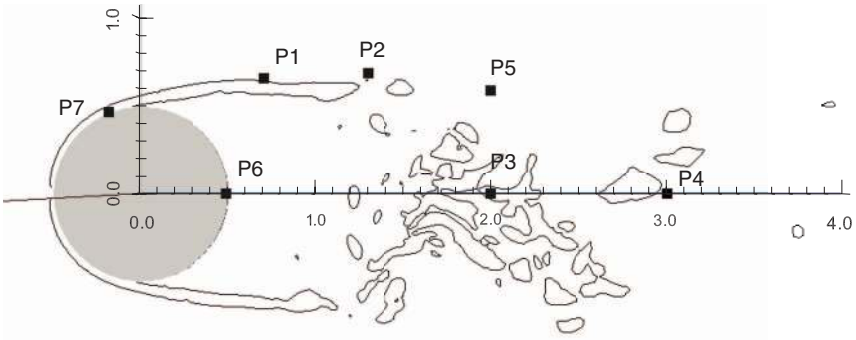

FIG. 1. Location of the computational probes.

TABLE I. Statistical flow features. DNS results compared with experimental measurements and numerical results from literature.

	L_z/D	Shedding cycles	f_{vs}	φ_s (°)	L_r/D	$\overline{C_d}$	$-\overline{C_{pb}}$
Present work	π	858	0.215	88	1.36	1.015	0.935
Present work, Mode L	π	250	0.218	87.8	1.55	0.979	0.877
Present work, Mode H	π	250	0.214	88.25	1.26	1.043	0.98
Parnaudeau *et al.*[12]	23	250	0.208	88	1.51	...	...
Norberg[30] ($Re = 3000$)	67	...	0.22	...	1.66	0.98[a]	0.88[a]
Lourenco and Shih[b]	21?		...	85	...	0.98	0.9
Dong *et al.*[31] ($Re = 4000$)	11.7	50	...	...	1.47	...	...
Ma *et al.*[11] (Case I) (DNS)	2π	100	0.203	...	1.12	0.96	0.96
Ma *et al.*[11] (Case II) (DNS)	π	100	0.219	...	1.59	0.84	0.88
Tremblay[32] (DNS)	π	50	0.22	85.7	1.3	1.03	0.93
Breuer[13] (LES)	π	~22	0.215	87.4	1.372	1.016	0.941
Kravchenko and Moin[14] (LES)	π	7	0.21	88	1.35	1.04	0.94
Franke and Frank[15] (LES)	π	40	0.209	88.2	1.64	0.978	0.85
Mahesh *et al.*[33] (LES)	π	33	0.218	87.6	1.35	1.0	...
Mani *et al.*[34] (LES)	π	60	0.206	86.3	...	0.99	0.86

[a]Taken from Kravchenko and Moin[14] at $Re = 4020$.
[b]Data summarised in Mittal.[35]

spectrum of the probes $P1$, $P2$, $P3$, and $P5$ by using the Lomb periodogram technique.[29] The resulting spectra have also been averaged in the span-wise direction. A segment of the time-series for the stream-wise and cross-stream velocity components are plotted in Figures 2 and 3, respectively. Their corresponding energy spectra are also depicted.

At all stations, the spectrum exhibits a dominant peak at $f_{vs} = 0.2145$ (all frequencies reported in this paper are in non-dimensional form), with the exception of the stream-wise spectrum of the probe located in the wake centreline ($P3$) in which its second-harmonic is visible ($f = 0.429$). The peak at f_{vs}, which corresponds with the large-scale vortex shedding frequency, is in agreement with the values reported in the literature (see Table I for more details). In addition, a broadband peak at a larger frequency and centred at $f_{KH} = 1.34$ is also detected. This peak corresponds with the Kelvin-Helmholtz instabilities of the separating shear-layer. This value is in fair agreement with Prasad and Williamson[7] predictions for this Reynolds number ($f_{KH} = 0.0235 Re^{0.67} f_{vs} = 1.29$). This secondary peak is only observed in the probes located at the shear-layers. Although at $P2$ ($x/D = 1.3$) is still visible in the cross-stream velocity fluctuations spectrum, its intensity diminishes as the flow moves downstream and is smeared out in the background of fluctuations of the turbulent flow.

On the top of both the vortex-shedding and the KH instabilities frequencies, there is also a peak at a much lower frequency than that of the vortex shedding ($f_{vs}/f_m = 33.5$). This peak occurs on average at $f_m = 0.0064$ and is also observed at almost every station located in the vortex formation zone. This frequency peak can clearly be seen in Figure 4 where a segment of the energy spectra of cross-stream velocity fluctuations at the shear-layer ($x/D = 0.71$; $y/D = 0.66$) and stream-wise of velocity fluctuations at the wake centreline ($x/D = 2.0$; $y/D = 0.0$) are depicted for the low frequencies. In both locations, the energy content at this low-frequency is quite large, even if it is compared to the energy content at the vortex shedding frequency (see Figure 4(a)). In fact, if the time series of the stream-wise velocity component at P3 is inspected (see Figure 2(e)), one can notice an almost periodic wave in the fluctuations of the variable with a frequency which is quite lower than that of the vortex shedding. This probe is located just after the closure of the mean recirculation bubble. This large-scale almost periodic motion registered points to the existence of a modulation of the vortex formation zone which causes its shrinking and enlargement over time. Note also the correspondence between the periods where stream-wise velocity at P3 is positive (Figure 2(e)), with the largest fluctuations in the cross-stream velocity registered at P1 probe (at the shear-layer, Figure 3(a)) for example, between $tU/D = 500$ and $tU/D = 550$. These alternating

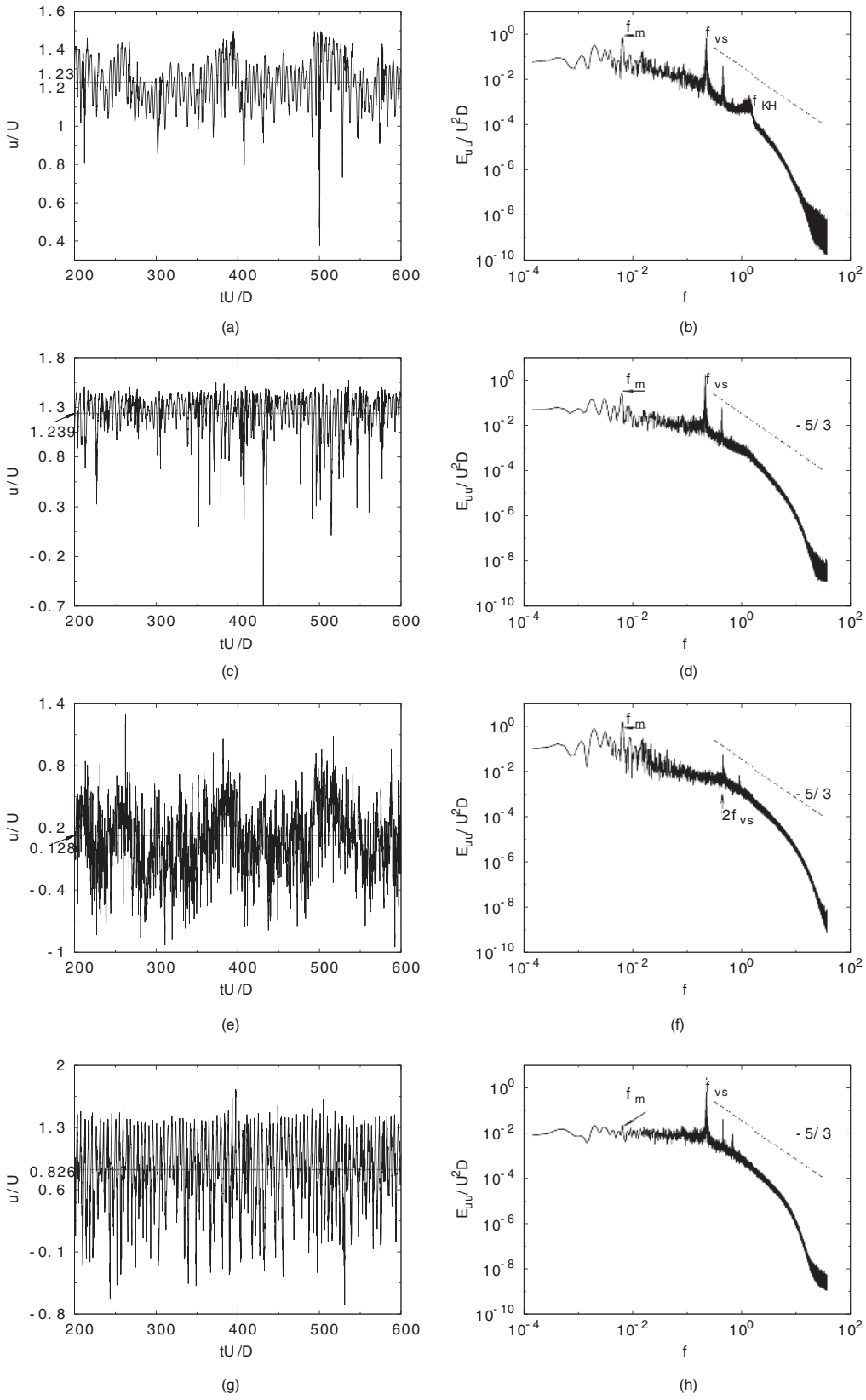

FIG. 2. Time history of the stream-wise velocity and its power spectrum at different locations: (a) and (b) at P1; (c) and (d) at P2; (e) and (f) at P3; and (g) and (h) at P5.

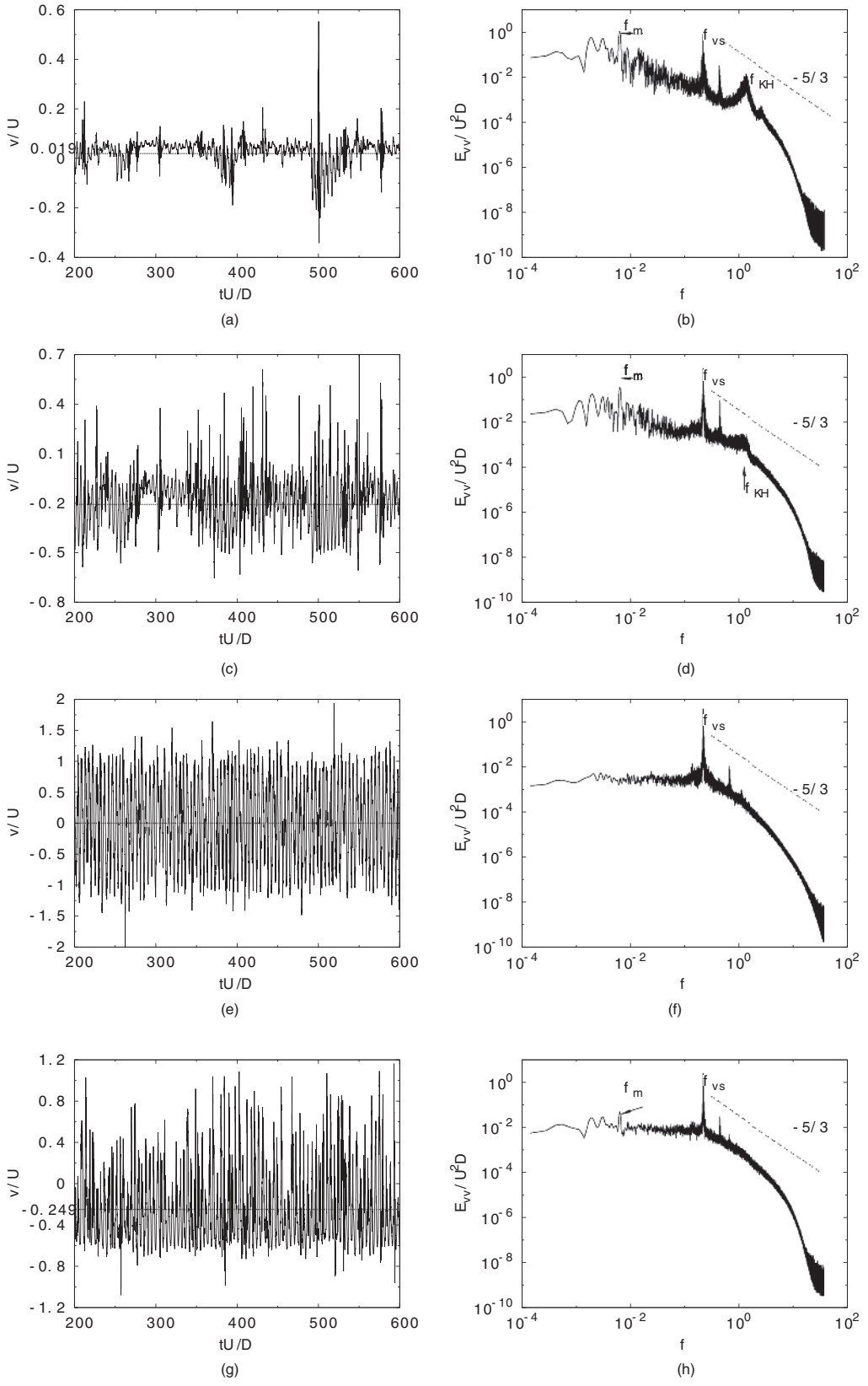

FIG. 3. Time history of the cross-stream velocity and its power spectrum at different locations: (a) and (b) at P1; (c) and (d) at P2; (e) and (f) at P3; and (g) and (h) at P5.

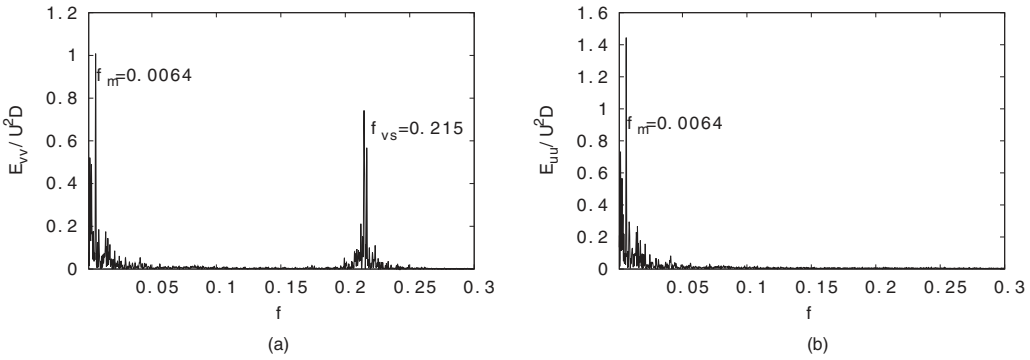

FIG. 4. Energy spectra of the (a) cross-stream velocity at [0.71,0.66] and (b) stream-wise velocity at [2.0,0.0].

periods of fluctuations of the cross-stream velocity in the shear-layer are what Prasad and Williamson[5] identified as intermittencies in the shear-layer.

With the analysis of the power spectra at different locations in the formation zone, some questions arise: is this low-frequency observed related with some modulation movement of the recirculation bubble? If this is the case, is there a relation between this movement and the base pressure? How does this shrinking and enlargement of the recirculation zone affect the topology of the wake and thus, the statistics in the vortex formation zone? Hereafter, we will try to answer these questions by analysing the instantaneous and average flow in the wake.

One way to analyse if two signals are correlated is by computing the cross-correlation between them. This should provide a measure of the rate at which one signal is affected by the information of the other. Here, correlations have been used to quantify the relation between the base-pressure fluctuations (taken at $P5$) and the stream-wise velocity fluctuations in the wake centreline (taken at $P3$). Note that $P3$ is located just after the closure of the mean recirculation bubble which occurs at $x/D = 1.86$. When this probe registers negative or close to zero values during a certain time period, this is indicative of the enlargement of the recirculation region, whereas the opposite represents a shrinkage of this region. Segments of the time series of both quantities, together with partially averaged signals (every 5 vortex shedding cycles) are plotted in Figures 5(a) and 5(b). If the signals are correlated one would expect high coherence between them with some frequency. The correlation, at τ time lag, of two time series ($\phi_1(t)$ and $\phi_2(t)$) can be defined as

$$\rho(\tau) = \frac{\langle \phi_1'(t)\phi_2'(t+\tau)\rangle}{\langle \phi_1'(t)^2\rangle^2 \langle \phi_2'(t)^2\rangle^2}, \tag{1}$$

where fluctuations of the variables are defined as $\phi'(t) = \phi(t) - \overline{\phi}$, being $\overline{\phi}$ the mean value at the probe location.

The resulting cross-correlation coefficients are plotted in Figure 5(c). In the figure, a well-defined periodic oscillation with a period (on average) of $\mathcal{T} = 156\ tU/D$ can be observed. This period matches the frequency ($f_m = 0.0064$) measured in the spectrum at different stations, which seems to be the footprint of the almost periodic wave motion observed in the stream-wise velocity at $P3$. The cross-correlation starts in a negative value, which might be interpreted as 180° phase angle between both signals. That is, as the base pressure gets more negative (see for instance Figure 5(b) at $tU/D \sim 700$), the stream-wise velocity at the wake centreline increases (Figure 5(a)), which points out the shrinking of the recirculation region and thus, of the vortex formation zone. On the contrary, as the base pressure gets less negative, the stream-wise velocity at $P3$ decreases meaning a lengthening of this zone.

This process is shown in Figure 6, where the visualisation of the instantaneous flow at two different vortex shedding cycles marked in Figures 5(a) and 5(b) as L and H, are depicted. Indeed, the point labelled as L corresponds with a time period in which the vortex formation zone gets longer (see Figure 6(a)), whereas the point marked as H is related with a shorter vortex formation zone (see Figure 6(b)).

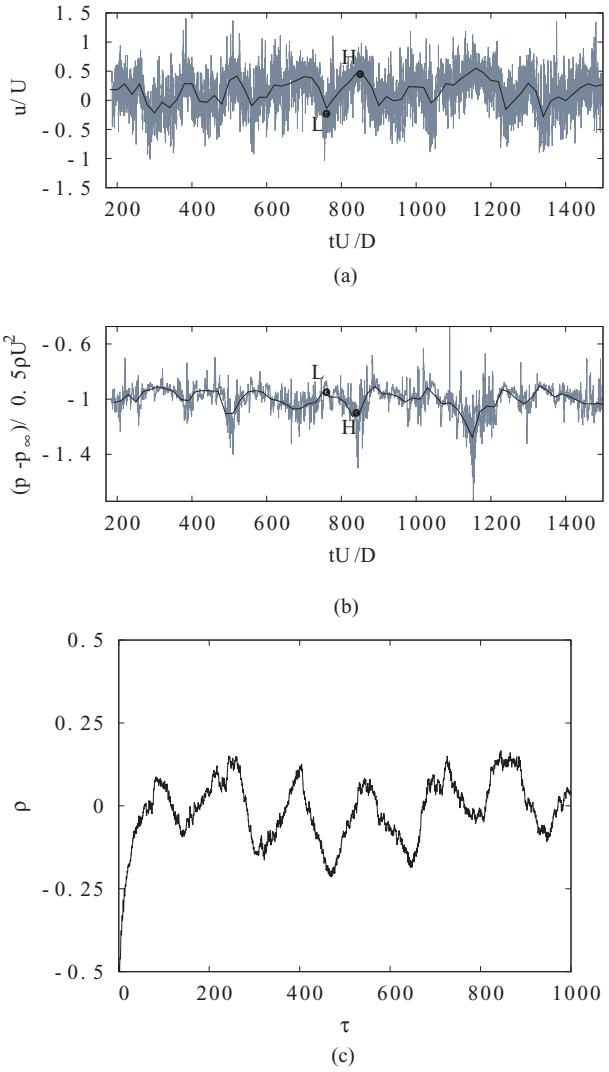

FIG. 5. (a) Time series of the velocity at *P*3, (b) time series of the base pressure *P*5, and (c) cross-correlation between the base pressure (*P*5) and stream-wise velocity fluctuations at *P*3 station.

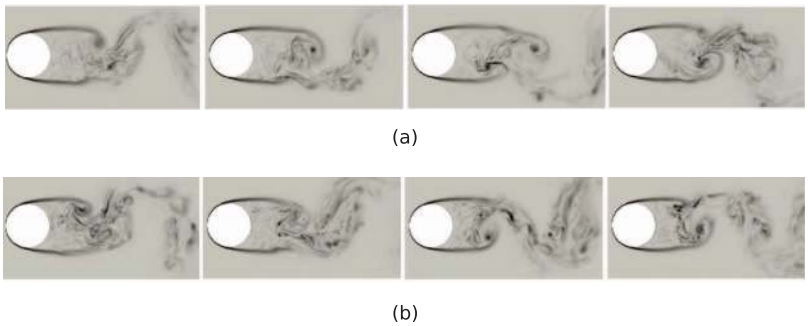

FIG. 6. Instantaneous vorticity: (a) larger vortex formation region, point L in Figure 5(a); and (b) shorter vortex formation region, point H in Figure 5(a).

The inverse correlation observed between the base pressure and the vortex formation length in the flow past bluff bodies as a function of the Reynolds number is a well known phenomenon, which has been the object of different studies (e.g., see Ref. 36). However, their correlation in the unsteady flow has received lesser attention. For higher Reynolds numbers, $Re > 2 \times 10^4$, Miau *et al*.[22] measured correlations between base pressure and velocity fluctuations for a trapezoidal and a circular cylinder. These correlations were of a time scale an order of magnitude larger than that of the vortex shedding. However, the implications of these low-frequency oscillations of the vortex formation zone in the wake topology have not yet been analysed.

B. Averaged statistics in the wake

The existence of different states in the near wake zone behind a normal flat plate was studied by Najjar and Balachandar.[21] Similar fluctuations in the recirculation zone behind bluff-bodies such as a circular disk or a sphere were also observed experimentally and numerically.[18,20,22] The low-frequency behaviour of the velocity fluctuations within the recirculation zone can be physically interpreted as the wake variation between two different modes: (i) a high-energy mode dominated by strong fluctuations in the shear-layer, and in general, large-amplitude fluctuations in the vortex formation zone, and (ii) a low-energy mode with weaker fluctuations in the shear layer. The large-amplitude fluctuations in the shear layers are accompanied with a shrinkage of the recirculation region, while when weaker fluctuations are observed there is also an enlargement of the recirculation region behind the cylinder. In fact, the correlation between the strong fluctuations of the flow within the recirculation region with the shortening of this zone was identified as a nonlinear effect by Zielinska *et al*.[37] Furthermore, as has been previously shown, there is also a linkage with the suction base pressure: the higher the value of the suction base pressure, the larger the vortex formation zone.

In order to analyse the wake configuration, we have computed partial time-average statistics when there is a shortening in the vortex formation region and when this zone experiences a lengthening process. To do this, the low-pass filtered signal of the stream-wise velocity at $P3$ station, with a cut-off frequency lower than that of the vortex-shedding, has been used as reference. Positive values of the periodic component of the resulting filtered velocity ($\tilde{u}_i > 0$) are expected when fluctuations are the largest. On the contrary, negative values of this quantity ($\tilde{u}_i < 0$) are expected when the observed fluctuations are weaker. With this criteria, segments of at least 10 consecutive vortex-shedding periods within each of these modes have been found throughout the whole calculation time (yielding a total of 250 shedding cycles), averaged, and their statistics computed. Following the same nomenclature as in Najjar and Balachandar,[21] the highest energetic mode (short recirculation) will be hereafter referred as Mode H, whereas the reference to Mode L will be used for the lower energetic mode (larger recirculation zone). In addition to the statistics computed for each mode, statistics for the whole time integration period (∼4000 TU) have also been evaluated. It should be pointed out that the statistics presented in this section have also been averaged in the span-wise direction.

The resulting time-averaged flow parameters are summarised in Table I. Besides the vortex shedding frequency previously commented, the separation angle (φ_s), recirculation length (L_r/D), drag coefficient (C_D), and base-pressure coefficient (C_{pb}) are presented. For comparison, experimental and numerical (from DNS and LES) results from the literature are also given. The computed flow parameters are in good agreement with the ones published by other researchers. In fact, the main differences registered are in the length of the recirculation bubble as one could expect.

The angular distribution of the mean pressure coefficient (Cp) for both modes and for the long-term averaged solution are plotted in Figure 7. Together with the present results, the pressure distribution measured by Norberg[6] at $Re = 3000$ and $Re = 3900$ are also shown. The result which better matches the experiments from Norberg is the solution corresponding with Mode L (larger vortex formation region). All three solutions collapse into the same curve in the laminar boundary layer up to a location somewhat upstream of the position where pressure reaches its minimum value (∼70°). After this location, the distribution corresponding with the lowest values of pressure occurs within Mode H, while long-term averaged solution is in between the two extreme modes. Note also the differences in the suction base pressure.

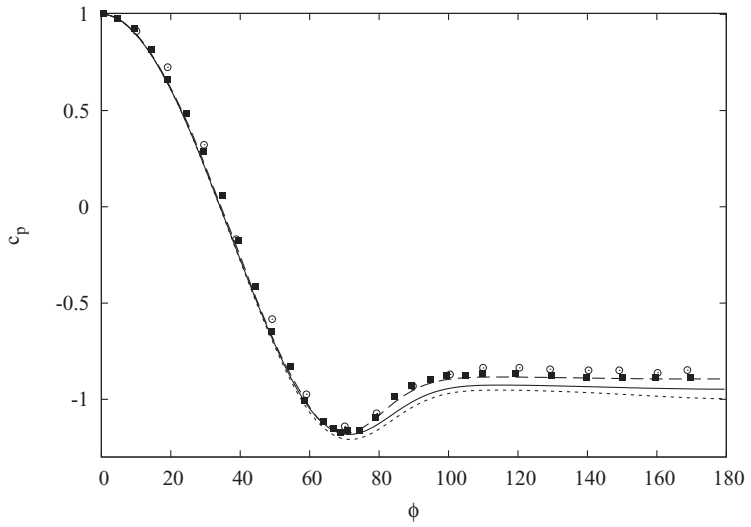

FIG. 7. Mean profiles distributions around the cylinder surface. Mean pressure distribution on the cylinder surface compared with experimental results: (solid squares) at $Re = 3900$, Norberg measurements taken from Kravchenko and Moin;[14] (circles) at $Re = 3000$ by Norberg;[6] (solid line) long-term averaged solution; (dotted line) Mode H; and (dashed line) Mode L.

In Figure 8, the stream-wise velocity profile and its fluctuations along the wake centreline are depicted. In the figure, the averaged values for both modes together with the long-term averaged solution are plotted. As can be observed, the profiles of stream-wise velocity and its fluctuations are quite different for each mode. The recirculation zone goes from $L_r/D = 1.26$ during Mode H to a larger value of $L_r/D = 1.55$ in Mode L. The long-term average solution (with ∼4000 time-units) is within both modes yielding a length of the recirculation region of $L_r/D = 1.36$. It is interesting to remark that this result is in good agreement with the value calculated by Kravchenko and Moin[14] (see Table I). In their LES, statistics were computed only over 35 time-units which is a very short integration time, considering the present results. One can conjecture that their averaging time was taken in the middle of both modes yielding a result quite close to the long-term averaged solution. This fact might be seen as fortuitous, as it could led to erroneous conclusions about the integration time required for obtaining converged statistics in the near wake.

From Figure 8(a), it can also be observed that the velocity deficit in Mode H is lower than in Mode L. This value is $u_{min}/U_{ref} = -0.23$ in mode H, while in mode L the stream-wise velocity in the wake centreline gets more negative ($u_{min}/U_{ref} = -0.32$). The position where this minimum occurs moves downstream, from $x/D = 1.35$ in mode H to $x/D = 1.59$ in mode L. However, it is

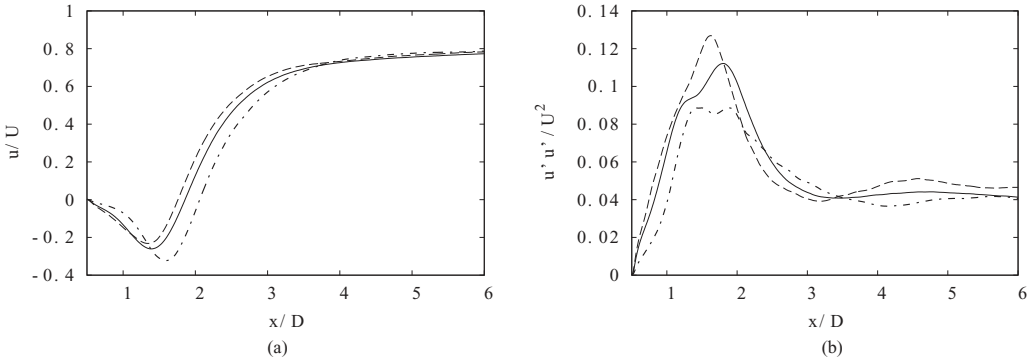

FIG. 8. Effects of the recirculation in the wake configuration: (a) averaged stream-wise velocity and (b) its averaged fluctuation along the wake centreline. (Solid line) Long-term averaged solution; (dashed line) Mode H; and (dash dotted line) Mode L.

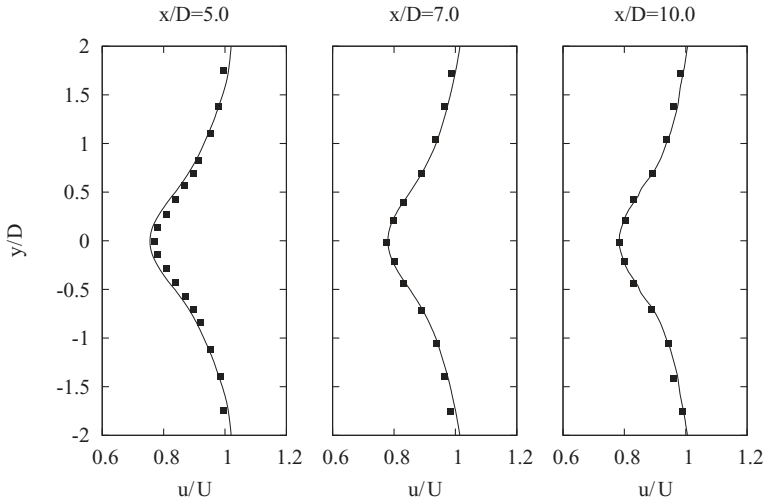

FIG. 9. Stream-wise velocity profile at different locations in the wake: (solid line) long-term averaged solution, and (solid squares) experimental results from Ong and Wallace.[38]

remarkable the fact that this behaviour is just restricted to the vortex formation zone, as the wake recovers after $x/D > 4$. This behaviour was also pointed out by Ma *et al.*[11] when compared the experimental data from Lourenco and Shih and Ong and Wallace.[38] Indeed, further downstream the profile of the long-term averaged solution compares quite well with the experimental results by Ong and Wallace[38] (see Figure 9).

Another striking fact is the profile of the stream-wise velocity fluctuations u_{rms} along the wake centreline (see Figure 8(b)). In Mode L, it exhibits a two-lobed peak with maximums at $x/D = 1.45$ and $x/D = 1.9$. The second one occurs just upstream of the location of the recirculation closure ($x/D = 1.95$). This profile is similar to that observed by Norberg[30] for $Re = 3000$. In his work, two peaks at $x/D = 1.4$ and $x/D = 2.1$ in the u_{rms} profile were identified. On the contrary, u_{rms} along the wake centreline in Mode H is quite different with only one peak at $x/D = 1.62$. Furthermore, Mode H presents a higher level of fluctuation, suggesting that it is more energetic and turbulent than Mode L. Moreover, u_{rms} profile for the long-term averaged solution is similar to that described by Norberg[39] for $Re > 8000$. This solution presents a peak at $x/D = 1.8$ and (what Norberg called) an inflection point upstream this peak, between $1.2 < x/D < 1.4$.

As has been commented before, in the literature there is a large scattering in the mean flow solutions in the near wake. This have been traditionally identified as different mean flow configurations of the stream-wise velocity and referred to as U-shape and V-shape profiles. Different causes for these contradictory results have been indicated in the literature, such as insufficient span-size of the domain, dissipative numerical schemes (in the case of DNS or LES solutions), or insufficient grid resolution in the shear-layers (see for instance Refs. 11 and 40). However, in the light of the results presented up until now, one can argue that these differences registered are due to the almost periodic modulation of the vortex formation zone observed as a shrinking and an enlargement of the recirculation. This unsteady long term motion of the near wake seems to be the cause of the different configurations observed.

In order to gain more insight into the behaviour of both modes, the stream-wise velocity profile and its fluctuations are plotted at different locations in the near wake at $x/D = 1.06$, $x/D = 1.54$, and $x/D = 2.02$ (Figure 10). For comparison, the solutions for each mode are plotted together with the experimental results from Parnaudeau *et al.*[12] and the numerical results of Case I from Ma *et al.*[11] (finer grid and larger span-wise domain). These reference solutions have been selected as both of them point out contradictory wake statistics due to their differences in the recirculation zone ($L_r/D = 1.51$ and $L_r/D = 1.12$, respectively). Also as reference, the long-term averaged solution is included (solid line in all plots).

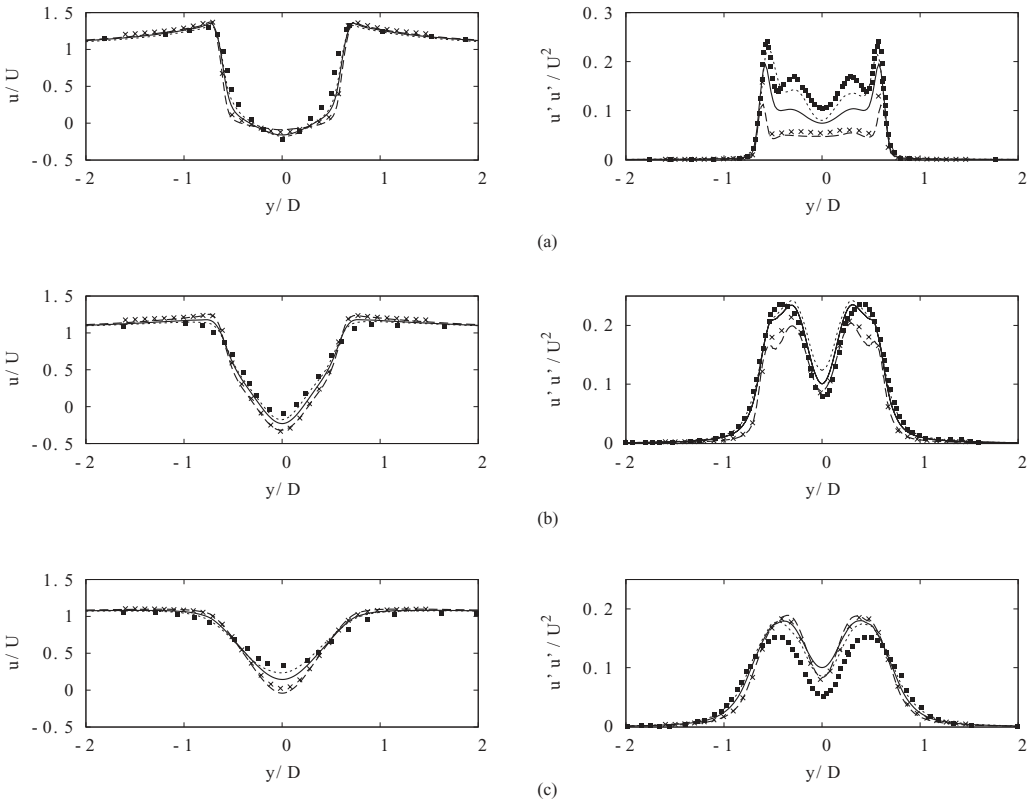

FIG. 10. Effects of the recirculation in the wake configuration and comparison with literature results. (Left) Averaged stream-wise velocity profile and (right) its fluctuation at different stream-wise locations: (a) $x/D = 1.06$; (b) $x/D = 1.54$; and (c) $x/D = 2.02$. (Solid line) Long-term averaged solution, (dotted line) Mode H; (dashed line) Mode L; (■) Case I from Ma *et al.*;[11] and (×) experimental results from Parnaudeau *et al.*[12]

As can be seen, there is a good agreement for first- and second-order statistics with both sets of data for each mode. Largest differences are observed with the solution from Ma *et al.*,[11] as in their case a shorter recirculation region was obtained (than that of Mode H presented in this work). The most energetic mode (Mode H) presents the largest fluctuations, especially in the region closest to the cylinder (at $x/D = 1.06$) where the stream-wise fluctuation peak at the shear layers is almost twice the value reached during Mode L. More differences between both modes are encountered if cross-flow velocity is compared at those locations (see Figure 11). Cross-flow velocity fluctuations peak at the wake centreline. In all measurement stations, Mode H is registered as more energetic than Mode L. Similar to the stream-wise velocity fluctuations, relative largest differences between both modes are attained in the closest location to the cylinder (at $x/D = 1.06$), where fluctuations in Mode H doubled the peak value of Mode L. However, in terms of absolute quantities, the cross-flow fluctuations increases as the flow approaches the recirculation bubble closure. For a more complete comparison of the near wake topology between both modes, in Figure 12 normal and shear Reynolds stresses are plotted. In the figure, the contour plots show the approximate location where these quantities reach a maximum. The exact position of these extrema are summarised in Table II, where they are compared to the long-term averaged solution. Note that as expected, for Mode H, Reynolds stresses peaks are the largest and occur at a position closer to the cylinder rear end, which confirms the modulation of the vortex formation zone. Note also that in spite of the relatively large integration time, asymmetries can still be observed in some of the quantities plotted. This is mainly due to the time required to achieve fully converged statistics.

It is clear that along the time, the flow past the cylinder experiences changes in the vortex formation region which affects the average statistics. Norberg[6] in his work, suggested that there is a change in the wake configuration at $Re = 5000$. This transition was later confirmed by Prasad and

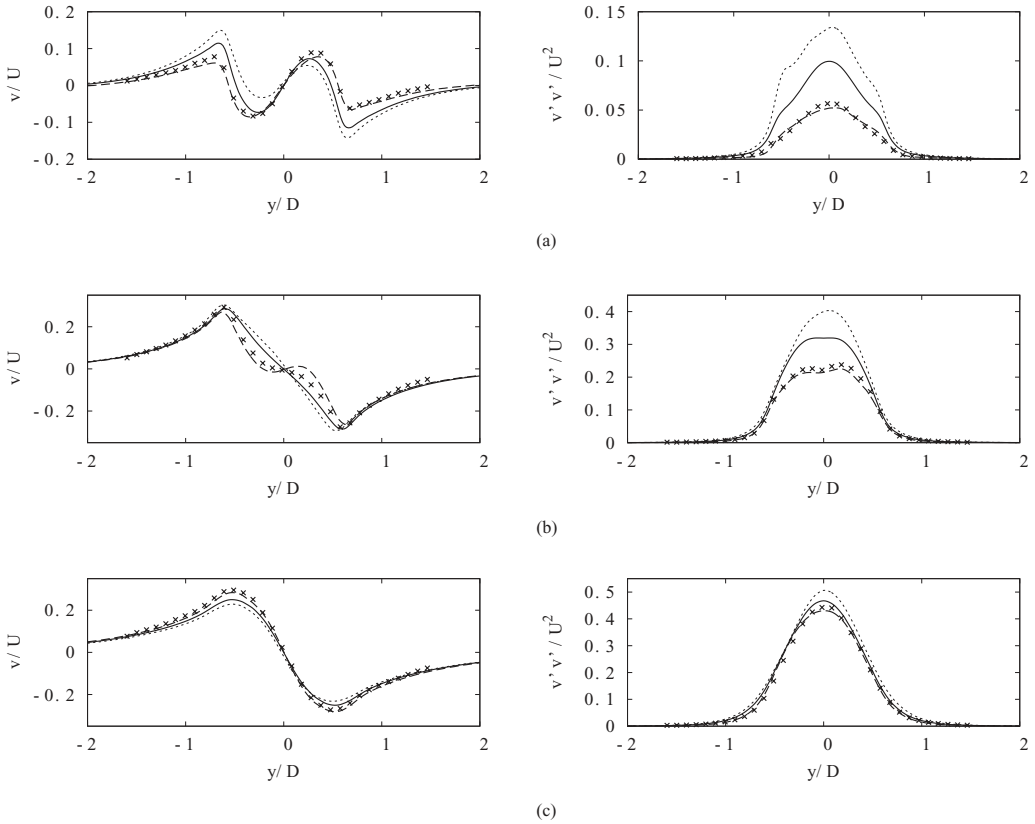

FIG. 11. Effects of the recirculation in the wake configuration and comparison with literature results when possible. (Left) Averaged cross-flow velocity profile and (right) its fluctuation at different stream-wise locations: (a) $x/D = 1.06$; (b) $x/D = 1.54$; and (c) $x/D = 2.02$. (Solid line) Long-term averaged solution, (dotted line) Mode H; (dashed line) Mode L; and (×) experimental results from Parnaudeau *et al.*[12]

Williamson,[41] while Norberg[39] attributed this change to a transition between a high- and low-quality vortex shedding mode. The results here presented suggest that at $Re = 3900$ both modes coexist and the wake is oscillating between them at a very low-frequency, and as has been shown this is the cause of the large scattering in the experimental and numerical results observed up until now. Norberg[39] suggested that the low-quality mode was the consequence of the loss of coherence in the

TABLE II. Minimum stream-wise velocity in the wake centreline and maximum values of the Reynolds stresses and turbulent kinetic energy (tke) for the different modes in comparison with the long-term averaged solution. The position of these quantities is also given.

	Long-term	Mode L	Mode H
$u_{\min}/U$	−0.261	−0.323	−0.233
(x/D,y/D)	(1.396,0)	(1.59,0)	(1.334,0)
$u'u'/U^2$	0.237	0.223	0.270
(x/D,y/D)	(1.576,±0.31)	(1.723,±0.298)	(1.489,±0.305)
$v'v'/U^2$	0.468	0.441	0.52
(x/D,y/D)	(2.00,0)	(2.105,0)	(1.922,0)
$u'v'/U^2$	−0.125	−0.126	−0.136
x/D,y/D)	(1.941,0.391)	(2.107,0.337)	(1.941,0.391)
tke/U^2	0.335	0.325	0.361
x/D,y/D)	(1.775,±0.216)	(1.924,±0.203)	(1.77,±0.199)

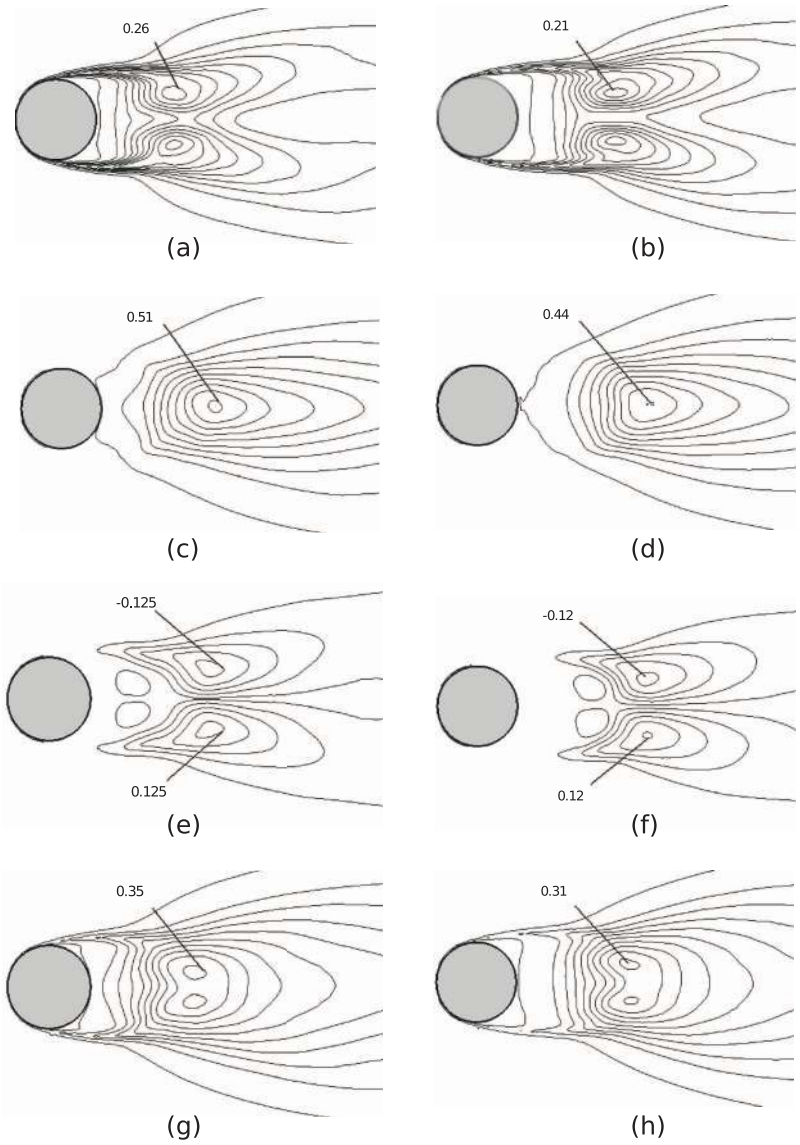

FIG. 12. Wake topology for both modes: Mode H ((a), (c), (e), (g)) and Mode L ((b), (d), (f), (h)). (a) and (b): stream-wise normal Reynolds stress; (c) and (d): cross-stream normal Reynolds stress; (e) and (f): shear Reynolds stress; and (g) and (h): turbulent kinetic energy. Each figure depicts 10 contour levels. Minimum level has been set to 0.01, except for the shear stress which is marked in the figure.

span-wise vortices, with vortex dislocations along the span. However, more study should be made in order to shed more light into the mechanism which triggers such oscillation.

C. Phase averaging

The mean flow of both modes is here analysed by means of the phase-average technique. The instantaneous flow can be represented by the contributions of a time-averaged component $\overline{\phi_i}$, a periodic fluctuation $\tilde{\phi}_i$ and a random fluctuation ϕ_i', i.e., $\phi_i = \overline{\phi_i} + \tilde{\phi}_i + \phi_i'$ (see Ref. 42). The phase-average can be defined as the average value of the variable ϕ_i over an ensemble of signals which have the same phase with respect to a reference signal. It can be evaluated as $\langle \phi_i \rangle = \overline{\phi_i} + \tilde{\phi}_i$. This decomposition opens the possibility of analysing the periodic motion of the flow by resolving the dominant frequency of the vortices.

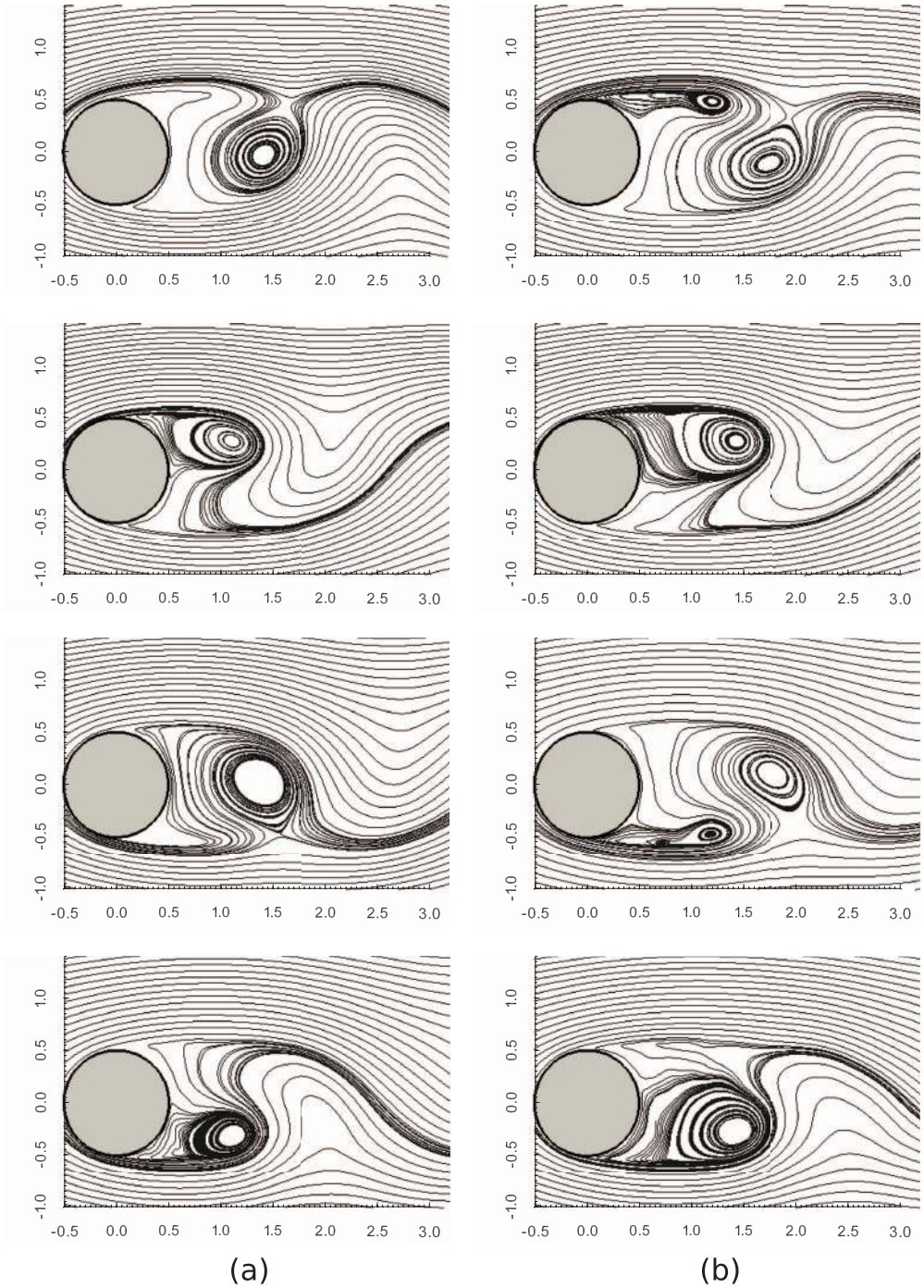

FIG. 13. Phase-averaged streamlines: (a) Mode H; and (b) Mode L.

For the ensemble average, 10 vortex shedding periods have been used to generate each coherent component. To do this, the pressure signal near the cylinder surface at probe station $P7$ (near the laminar boundary layer) has been used as the reference oscillator. In this position, the pressure signal varies in an almost periodic manner with a period equal to the vortex shedding. Streamlines and span-wise vorticity contours for both modes at phase angles of $\phi = 0^\circ,\ 90^\circ,\ 180^\circ$, and 270° are represented in Figure 13.

The vortex-shedding process in both modes is clearly captured. The wake topology is quite similar for both modes. Indeed, the wake topology remains qualitatively similar during the whole subcritical regime (see for instance Refs. 43 and 44). However, there are also some important differences between both wakes topologies. The first phase of the vortex shedding shows a saddle point which clearly marks the start of the new vortex. This saddle point can be located at $x/D = 1.6$; $y/D = 0.45$ in Mode H. For Mode L, it is located downstream and closest to the wake centreline at $x/D = 1.93$; $y/D = 0.35$. This is an important difference which points out the strength of the vortex shedding during Mode H if compared to Mode L. The strongest vortex shedding during Mode H produces the entrainment of the vortex core into the wake centreline, as can be seen by its position at $x/D = 1.4$; $y/D = 0.0$. This is in contrast with the location of the same vortex but during Mode L, which can be seen a slight downstream and off the wake centreline ($x/D = 1.75$; $y/D = -0.1$). Stream-wise normal and shear Reynolds stresses are maximum in the top shear layer near the position of the saddle point, whereas cross-stream normal Reynolds stress has two maximums near the position of the vortex core.

Phase angle (90°) shows the vortex completely formed near the top shear layer. Stream-wise fluctuations are maximum near the vortex core and due to the entrainment of the turbulent shear layer in the recirculation zone, cross-stream normal Reynolds stress experiences an increase near the position where the mean recirculation bubble closes. The two last phases of the vortex shedding describe a similar situation, but now the new vortex is forming in the bottom shear layer.

V. CONCLUDING REMARKS

The study of the wake configuration of the flow past a circular cylinder has been carried out by means of the DNS at $Re = 3900$. The analysis of the spectra of the velocity at different locations in the vortex formation zone, suggests that together with the vortex-shedding frequency and the small-scale Kelvin-Helmholtz instabilities frequency, there is also a low-frequency which can be attributed to the shrinkage and enlargement of the recirculation region. This low-frequency, measured from the analysis of several probes in the vortex formation region, is of $f_m = 0.0064$. This modulation of the recirculation zone can be seen as two alternating wake configurations which have been identified as (i) a high-energy mode with larger fluctuations in the shear-layer (Mode H) and (ii) a low-energy mode with weaker fluctuations in the shear layer (Mode L).

The large-amplitude fluctuations in the shear layers are accompanied with a shrinkage of the recirculation region, while when weaker fluctuations are observed there is also an enlargement of the recirculation region behind the cylinder. Furthermore, from the cross-correlation analysis between the pressure at the base of the cylinder and the stream-wise velocity at the wake centreline, it has been shown that both variables are inverse correlated. As the suction base pressure gets more negative, the stream-wise velocity increases and as a consequence, the vortex formation zone decreases. This unsteady motion of the vortex formation has a direct influence in the near wake statistics as a long integration time is required for obtaining converged statistics, if it is considered that alternating modes of the wake occurs every 156 time-units on average. This is the main cause of the large scattering of solutions registered in the literature. As has been shown, by accommodating the averaging period to each mode, it is possible to obtain partial statistics which compare quite well with previous experimental and DNS results.

TABLE III. Main parameters for the different computations: L_z, span-wise size; N_t, total number of CVs; $N_{CV\,plane}$, number of CVs in the plane; N_{planes}, number of planes in the homogeneous direction; and N_{BL}, number of points in the viscous boundary layer.

Case	L_z	$N_t[MCV]$	$N_{CV\,plane}$	N_{planes}	N_{BL}
I (present results)	πD	9.3	72700	128	10
II	$2\pi D$	18.6	72700	256	10
III	πD	1.62	50774	32	4

TABLE IV. Statistical flow parameters for the different grids.

	St	C_d	$-C_{pb}$	L_r/D
Case I (9.3 MCV)	0.215	1.015	0.935	1.36
Case II (18.6 MCV)	0.214	1.019	0.933	1.363
Case III (1.62 MCV)	0.218	1.05	0.94	1.35

In order to gain insight into the wake topology for each mode, phase average statistics have been also computed. Although the vortex shedding period of each mode is quite similar, important differences have been also pointed out. During Mode H, not only does the transition to turbulence occur closer to the cylinder and the vortex formation zone is shortened, but also vortices shed are aligned on the wake centreline, whereas in Mode L, the formed vortices remain slightly off the wake centreline.

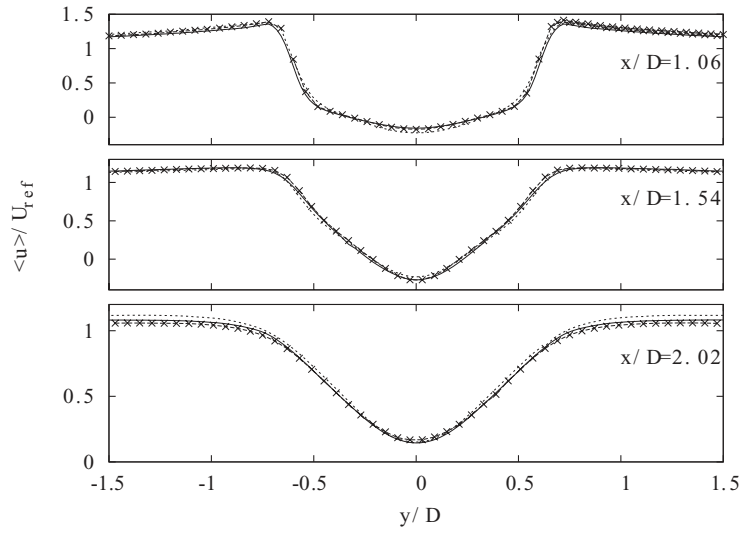

(a)

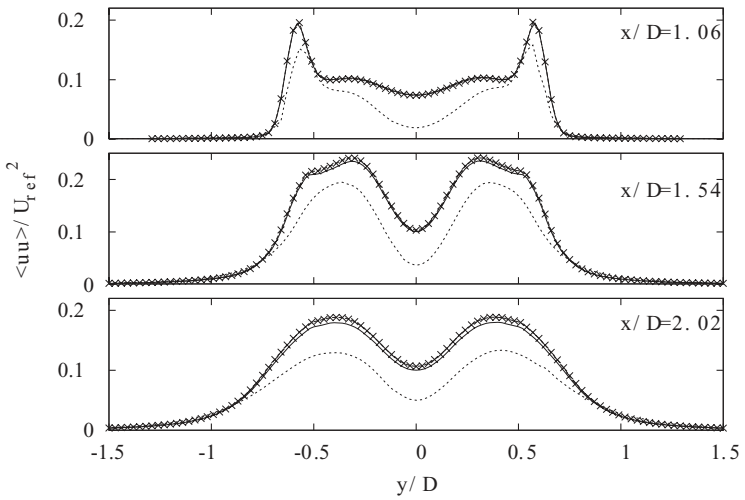

(b)

FIG. 14. Stream-wise velocity profile and its fluctuations at different locations in the near-wake for different grids resolutions: (solid line) case I; (-x-) case II; and (dotted line) case III.

ACKNOWLEDGMENTS

This work has been partially financially supported by the Ministerio de Economía y Competitividad, Secretaría de Estado de Investigación, Desarrollo e Innovación, Spain (ref. ENE2009-07689) and by the Collaboration Project between Universidad Politècnica de Catalunya and Termo Fluids S.L. We also acknowledge the computational resources at Marenostrum Supercomputer II granted by "Red Española de Supercomputación." The authors would like to sincerely acknowledge Philippe Parnaudeau, Johan Carlier, Dominique Heitz, and Eric Lamballais for providing their experimental data. The authors would also like to thank the referees for their useful comments which served to improve the paper.

APPENDIX A: GRID RESOLUTION STUDIES

Computations with different grid resolutions and different span-wise size have also been considered (see Table III). Even for the coarser grid, a minimum number of control volumes within

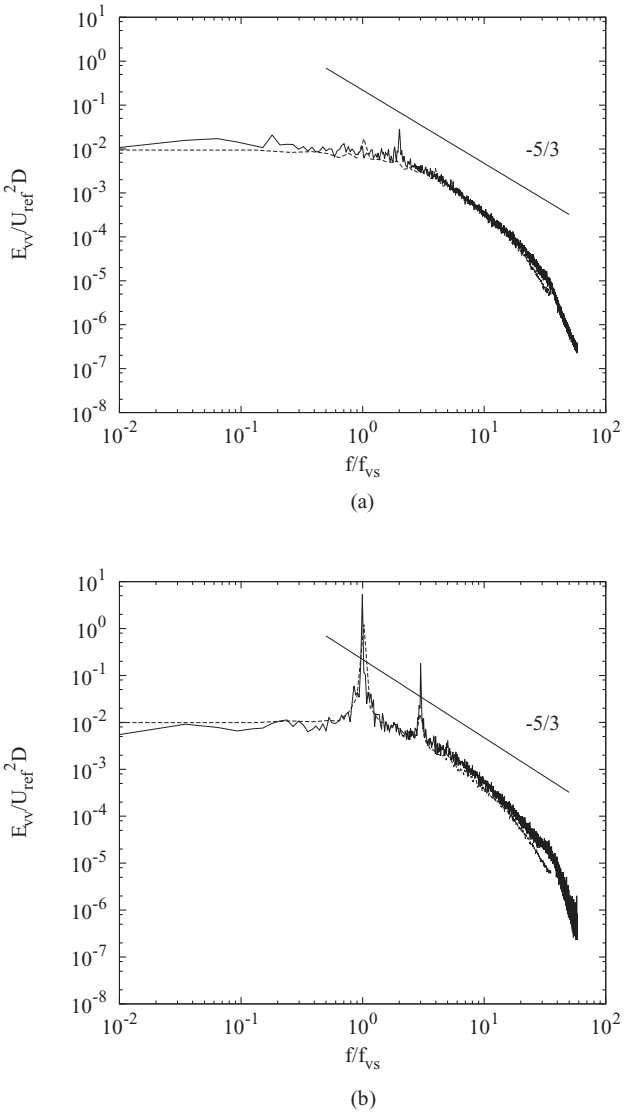

FIG. 15. Energy spectra of the stream-wise and cross-stream velocity fluctuations at probe *P*4 (solid line) for case I (see Table III). Comparison with experimental measurements by Parnaudeau *et al.*[12] (dashed line).

the boundary layer has been imposed. Main flow features resulting from all cases are summarised in Table IV. As temporal integration is of main concern in the present work, statistics have been computed for at least 1500 time-units and have been averaged in time and in the span-wise direction. As can be seen, in terms of averaged values, even with the coarser grid, a good agreement is obtained.

However, in order of perform a more detailed comparison, considering both first- and second-order statistics, the stream-wise velocity and its fluctuations at different location in the near wake have been compared. These results are shown in Figure 14. Although stream-wise velocity at these locations shows a good agreement for all grids, larger differences are obtained with the coarse one for the second-order statistics. However, when comparing the velocity fluctuations for cases I and II in Figure 14(b) (span-wise size $L_z = \pi D$ and $L_z = 2\pi D$, respectively), almost no noticeable differences can be observed.

APPENDIX B: COMPARISON OF ENERGY SPECTRA

The stream-wise and cross-flow velocity fluctuations spectra at the wake centreline (at probe $P4$, $x/D = 3$) obtained with case I grid are compared with the experimental data from Parnaudeau *et al.*[12] The resulting comparison is depicted in Figure 15. Note the good agreement between both results at all frequencies. It is very remarkable how the numerical data fit the experimental cross velocity spectra for the peaks of the fundamental frequency ($f/f_{vs} = 1$) and its third harmonic ($f/f_{vs} = 3$), which are very pronounced. Unfortunately for the spectra of stream-wise velocity, the same level of consistency in the fundamental peak is no longer obtained. DNS data predict a pronounced peak at the second harmonic of the vortex-shedding frequency for the stream-wise spectrum as expected for a probe located in the wake centreline. However, Parnaudeau *et al.*[12] indicated the occurrence of a peak in the u-spectra at the vortex shedding frequency due to the cosine law and calibration methods used in their Hot Wire Anemometry (HWA) measurements, which lead to slight contaminations of their results.

[1] A. Roshko, "On the development of turbulent wakes from vortex streets," Technical Report No. NACA TR 1191 (California Institute of Technology, 1953).
[2] M. S. Bloor, "The transition to turbulence in the wake of a circular cylinder," J. Fluid Mech. **19**, 290–304 (1964).
[3] C. H. K. Williamson, "The existence of two stages in the transition to three dimensionality of a cylinder wake," Phys. Fluids **31**, 3165–3168 (1988).
[4] C. H. K. Williamson, "Vortex dynamics in the cylinder wake," Annu. Rev. Fluid Mech. **28**, 477–539 (1996).
[5] A. Prasad and C. H. K. Williamson, "The instability of the separated shear layer from a bluff body," Phys. Fluids **8**, 1347 (1996).
[6] C. Norberg, "Effects of Reynolds number and a low intensity free-stream turbulence on the flow around a circular cylinder," Technical Report, Publication No. 87/2 (Department of Applied Thermodynamics and Fluid Mechanics, Chalmers University of Technology, Sweden, 1987).
[7] A. Prasad and C. H. K. Williamson, "The instability of the shear layer separating from a bluff body," J. Fluid Mech. **333**, 375–492 (1997).
[8] A. Roshko, "Experiments on the flow past a circular cylinder at very high Reynolds number," J. Fluid Mech. **10**, 345–356 (1961).
[9] P. W. Bearman, "Investigation of the flow behind a two-dimensional model with a blunt trailing edge and fitted with splitter plates," J. Fluid Mech. **21**, 241–255 (1965).
[10] G. Schewe, "On the force fluctuations acting on a circular cylinder in crossflow from subcritical up to transcritical Reynolds numbers," J. Fluid Mech. **133**, 265–285 (1983).
[11] X. Ma, G. S. Karamanos, and G. E. Karniadakis, "Dynamics and low-dimensionality of a turbulent wake," J. Fluid Mech. **410**, 29–65 (2000).
[12] P. Parnaudeau, J. Carlier, D. Heitz, and E. Lamballais, "Experimental and numerical studies of the flow over a circular cylinder at Reynolds number 3900," Phys. Fluids **20**, 085101 (2008).
[13] M. Breuer, "Large eddy simulation of the subcritical flow past a circular cylinder: Numerical and modeling aspects," Int. J. Numer. Methods Fluids **28**, 1281–1302 (1998).
[14] A. G. Kravchenko and P. Moin, "Numerical studies of flow over a circular cylinder at $Re_D = 3900$," Phys. Fluids **12**, 403–417 (2000).
[15] J. Franke and W. Frank, "Large eddy simulation of the flow past a circular cylinder at $Re_D = 3900$," J. Wind. Eng. Ind. Aerodyn. **90**, 1191–1206 (2002).
[16] F. Tremblay, M. Manhart, and R. Friedrich, "LES of flow around a circular cylinder at a subcritical Reynolds number with Cartesian grids," Fluid Mech. A **65**, 133–150 (2004).
[17] M. S. Bloor and J. H. Gerrard, "Measurements on turbulent vortices in a cylinder wake," Philos. Trans. R. Soc. London, Ser. A **294**, 319–342 (1966).

[18] E. Berger, D. Scholz, and M. Schumm, "Coherent vortex structures in the wake of a sphere and a circular disk at rest and under forced vibrations," J. Fluid Struct. **4**, 231–257 (1990).
[19] A. Tomboulides and S. A. Orszag, "Numerical investigation of transitional and weak turbulent flow past a sphere," J. Fluid Mech. **416**, 45–73 (2000).
[20] I. Rodríguez, R. Borrell, O. Lehmkuhl, C. D. Pérez-Segarra, and A. Oliva, "Direct numerical simulation of the flow over a sphere at Re = 3700," J. Fluid Mech. **679**, 263–287 (2011).
[21] F. M. Najjar and S. Balachandar, "Low-frequency unsteadiness in the wake of a normal flat plate," J. Fluid Mech. **370**, 101–147 (1998).
[22] J. J. Miau, J. T. Wang, J. H. Chou, and C. Y. Wei, "Characteristics of the low-frequency variations embedded in vortex shedding process," J. Fluid Struct. **13**, 339–359 (1999).
[23] S. J. Wu, J. J. Miau, C. C. Hu, and J. H. Chou, "On low-frequency modulations and three-dimensionality in vortex shedding behind a normal plate," J. Fluid Mech. **526**, 117–146 (2005).
[24] I. Rodríguez, O. Lehmkuhl, R. Borrell, and A. Oliva, "Flow dynamics in the wake of a sphere at sub-critical Reynolds numbers," Comput. Fluids **80**, 233–243 (2013).
[25] R. W. C. P. Verstappen and A. E. P. Veldman, "Symmetry-preserving discretization of turbulent flow," J. Comput. Phys. **187**, 343–368 (2003).
[26] F. X. Trias and O. Lehmkuhl, "A self-adaptive strategy for the time integration of Navier-Stokes equations," Numer. Heat Transfer, Part B **60**, 116–134 (2011).
[27] R. Borrell, O. Lehmkuhl, F. X. Trias, and A. Oliva, "Parallel direct Poisson solver for discretisations with one Fourier diagonalisable direction," J. Comput. Phys. **230**, 4723–4741 (2011).
[28] O. Lehmkuhl, R. Borrell, J. Chivas, and C. D. Perez-Segarra, "Direct numerical simulations and symmetry-preserving regularization simulations of the flow over a circular cylinder at Reynolds number 3900," in *Turbulence, Heat and Mass Transfer 6*, edited by K. Hanjalic, K. Nagano, and S. Jakirlic (Begell House Inc., 2009), pp. 325–328.
[29] N. R. Lomb, "Least-squares frequency analysis of unequally spaced data," Astrophys. Space Sci. **39**, 447–462 (1976).
[30] C. Norberg, "LDV measurements in the near wake of a circular cylinder," in *Proceedings of the ASME Conference on Advances in the Understanding of Bluff Body Wakes and Vortex Induced Vibration*, (ASME, Washington D.C., 1988).
[31] S. Dong, G. E. Karniadakis, A. Ekmekci, and D. Rockwell, "A combined direct numerical simulation-particle image velocimetry study of the turbulent near wake," J. Fluid Mech. **569**, 185 (2006).
[32] F. Tremblay, "Direct and large-eddy simulation of flow around a circular cylinder at subcritical Reynolds numbers," Ph.D. thesis, Technische Universität München, 2002.
[33] K. Mahesh, G. Constantinescu, and P. Moin, "A numerical method for large-eddy simulation in complex geometries," J. Comput. Phys. **197**, 215–240 (2004).
[34] A. Mani, P. Moin, and M. Wang, "Computational study of optical distortions by separated shear layers and turbulent wakes," J. Fluid Mech. **625**, 273 (2009).
[35] R. Mittal, "Large eddy simulation of flow past a circular cylinder," CTR Annual Research Briefs (Center for Turbulence Research, 1995), pp. 107–116.
[36] M. F. Unal and D. Rockwell, "On vortex formation from a cylinder. Part 1. The initial instability," J. Fluid Mech. **190**, 491–512 (1988).
[37] B. J. A. Zielinska, S. Goujon-Durand, J. Dusek, and J. E. Wesfreid, "Strongly nonlinear effect in unstable wakes," Phys. Rev. Lett. **79**, 3893–3896 (1997).
[38] L. Ong and J. Wallace, "The velocity field of the turbulent very near wake of a circular cylinder," Exp. Fluids **20**, 441–453 (1996).
[39] C. Norberg, "Fluctuating lift on a circular cylinder: review and new measurements," J. Fluid Struct. **17**, 57–96 (2003).
[40] J. Wissink and W. Rodi, "Numerical study of the near wake of a circular cylinder," Int. J. Heat Fluid Flow **29**, 1060–1070 (2008).
[41] A. Prasad and C. H. K. Williamson, "Three-dimensional effects in turbulent bluff body wakes," J. Fluid Mech. **343**, 235–265 (1997).
[42] W. C. Reynolds and A. K. M. F. Hussain, "The mechanics of an organized wave in turbulent shear flow. Part 3. Theoretical models and comparisons with experiments," J. Fluid Mech. **54**, 263–288 (1972).
[43] B. Cantwell and D. Coles, "An experimental study of entrainment and transport in the turbulent near wake of a circular cylinder," J. Fluid Mech. **136**, 321–374 (1983).
[44] U. Ünal and M. Atlar, "An experimental investigation into the effect of vortex generators on the near-wake flow of a circular cylinder," Exp. Fluids **48**, 1059–1079 (2010).